

On the continuum radio-spectrum of Cas A: possible evidence of the non-linear particle acceleration

D. Onić¹

donic@matf.bg.ac.rs

and

D. Urošević^{1,2}

Received _____; accepted _____

¹Department of Astronomy, Faculty of Mathematics, University of Belgrade, Serbia

²Isaac Newton Institute of Chile, Yugoslavia Branch

ABSTRACT

Integrated radio-spectrum of Cas A in continuum was analyzed with special emphasis on possible high frequency spectral curvature. We conclude that the most probable scenario is that *Planck's* new data reveal the imprint of non-linear particle acceleration in the case of this young Galactic supernova remnant (SNR).

Subject headings: ISM: individual (Cas A) – radiation mechanisms: non-thermal – acceleration of particles – ISM: supernova remnants – radio continuum: ISM

1. Introduction

*Planck*¹ is the third generation space mission to measure the anisotropy of the cosmic microwave background. It observed the sky in nine frequency bands covering 30 - 857 GHz with high sensitivity and angular resolution from 5' to 31' (Arnaud et al. 2014 and references therein). The Low Frequency Instrument covers the 30, 44, and 70 GHz bands while the High Frequency Instrument covers the 100, 143, 217, 353, 545, and 857 GHz bands. *Planck's* sensitivity, angular resolution, and frequency coverage make it a powerful instrument for Galactic and extragalactic astrophysics as well as cosmology.

Cassiopeia A (Cas A) is a very bright and young supernova remnant (SNR), likely due to a historical supernova around 353 – 343 yr ago (Ashworth 1980; Fesen et al. 2006). Its estimated distance is 3.33 ± 0.10 kpc (Alarie et al. 2014). Recently, this SNR was observed by *Planck* and the results were published in Arnaud et al. (2014). It was shown that Cas A is a distinct compact source from 30 - 353 GHz but becomes confused with unrelated Galactic clouds at the highest *Planck* frequencies (545 and 857 GHz). The apparent excess radiation at 217 and 353 GHz is proposed to be due to coincidental peak in the unrelated foreground emission or to cool dust in the supernova remnant (Arnaud et al. 2014).

The slightly concave-up forms of radio-spectra were detected for some young SNRs (Reynolds & Ellison 1992). The main reason for high frequency concave-up curvature in radio-spectra of young SNRs should originate in non-linear diffuse shock particle acceleration (see Urošević 2014 and references therein). Due to positive identification of

¹*Planck* is a project of the European Space Agency (ESA) with instruments provided by two scientific consortia funded by ESA member states, with contributions from NASA (USA) and telescope reflectors provided by a collaboration between ESA and a scientific consortium led and funded by Denmark.

infrared synchrotron radiation from Cas A, Jones et al. (2003) gave indication that the radio-spectrum of this SNR should be concave-up.

This paper focuses on the analysis of origin of the high-frequency curvature in radio-spectrum of Cas A.

2. Analysis and Results

There are various observations of SNR Cas A (Green 2014). Flux densities at different frequencies for SNR Cas A were taken from different papers. Different samples for data analysis were used to account for differences in data gathered from various literature. The first sample includes data from Arnaud et al. (2014), Baars et al. (1977) and references therein as well as from Mason et al. (1999). The original data (data for original epochs) are taken from Table 2 of Baars et al. (1977), not the scaled ones. The second sample is formed by addition of data from Hurley-Walker et al. (2009) and Liszt & Lucas (1999). The frequency range for both samples is 0.55 - 353 GHz. The integrated flux density of 52 ± 7 Jy at 353 GHz was adopted in accordance with the discussion presented in Arnaud et al. (2014).

Before actual analysis, the flux densities were appropriately scaled to account for secular fading. The epoch (2010.0) is chosen to coincide with *Planck's* intermediate astrophysics results (Arnaud et al. 2014). Two scaling relations were used in this paper. The first one, commonly used, is taken from Baars et al. (1977) in the following form

$$\begin{aligned}
 d(\nu) &= a - b \log \nu_{[\text{GHz}]}, \\
 \Delta d(\nu) &= \Delta a + \Delta b |\log \nu_{[\text{GHz}]}|, \\
 a &= (0.0097 \pm 0.0004), \quad b = (0.003 \pm 0.0004),
 \end{aligned}
 \tag{1}$$

where $d(\nu)$ is the secular decrease in the flux density at given frequency and $\Delta d(\nu)$ is an

appropriate error estimate.

On the other hand, it was debated that this scaling relation is not appropriate (O’Sullivan & Green 1999) especially for the lowest radio-frequencies (Helmboldt & Kassim 2009 and references therein).

Due to the lack of accuracy of the above mentioned relation, the scaling proposed in Vinyaikĭn (2014) was also used in the following form

$$\begin{aligned}
 d(\nu) &= a - b \ln \nu_{[\text{GHz}]} - c \nu_{[\text{GHz}]}^{-2.1}, \\
 \Delta d(\nu) &= \Delta a + \Delta b |\ln \nu_{[\text{GHz}]}| + \Delta c \nu_{[\text{GHz}]}^{-2.1}, \\
 a &= (0.0063 \pm 0.0002), \quad b = (0.0004 \pm 0.0001), \\
 c &= (0.0151 \pm 0.0016) \times 10^{-5}.
 \end{aligned} \tag{2}$$

The results obtained analyzing data formed by these two scaling relation are compared.

The flux density for the desired epoch and the appropriate error estimate are calculated by

$$\begin{aligned}
 S_{t_2}(\nu) &= S_{t_1}(\nu) (1 - d(\nu))^T, \quad T = t_2 - t_1, \\
 \Delta S_{t_2}(\nu) &= S_{t_1}(\nu) \left(\frac{\Delta S_{t_1}(\nu)}{S_{t_1}(\nu)} + T \frac{\Delta d(\nu)}{1 - d(\nu)} \right).
 \end{aligned} \tag{3}$$

It is worth noting that radio-spectrum of Cas A shows low-frequency cut-off due to thermal absorption (Vinyaikĭn 2014) or possibly synchrotron self-absorption. As the main interest of this paper involves analysis of high frequency part of the Cas A radio-spectrum, first, only data at frequencies higher than around 550 MHz were analyzed (for both scaling relation).

To show that the observed high-frequency radio-spectrum of Cas A is actually curved, the principal component analysis (PCA) was first applied (Babu & Feigelson 1996). The

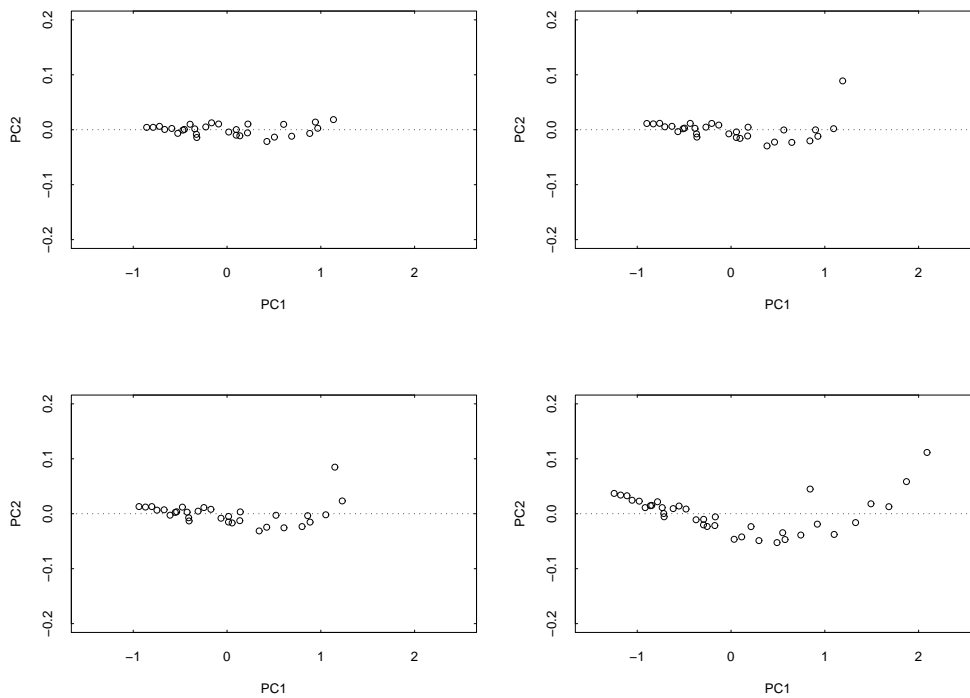


Fig. 1.— The results of PCA on data from the first sample. Scaling relation taken from Baars et al. (1977) was used. PC1 and PC2 correspond to the first and second principal component, respectively. In the upper left figure are the results of PCA on the radio-data between 550 MHz and 30 GHz. Departure from the linear relationship is obvious when the observation at 30 GHz is added (upper right figure), both data at 30 and 32 GHz are added (down left figure) and when the whole range of frequencies up to 353 GHz is used (down right figure)

principal components are the eigenvectors of the covariance matrix. Original data are represented in the basis formed by these vectors. The first principal component accounts for as much of the variability in the data as possible, i.e. it has the largest possible variance. The second principal component has the highest variance possible under the constraint that it is orthogonal to the first one. In that sense, PCA includes calculation of the highest data variability direction which can be used to detect departures from the pure power-law spectra (linear fit in log-log scale).

In Figure 1, the results of PCA on logarithmically transformed data ($\log \nu, \log S_\nu$) from the first sample are presented. PC1 and PC2 correspond to the first and second principal component, respectively. The plotted values represent the original data in the basis of principal components (zero centered data multiplied by the rotation matrix whose columns contain the eigenvectors). The covariance of these values represents a diagonal matrix with squares of standard deviations of the principal components eigenvalues as its elements. In the upper left figure are the results of PCA on the radio-data between 550 MHz and 30 GHz. It is clear that the radio-spectrum follows pure power-law relation. Addition of the observation at 30 GHz (upper right figure), both data at 30 and 32 GHz (down left figure) and if whole range of frequencies up to 353 GHz is analyzed (down right figure), shows that the radio-spectrum of Cas A is positively curved (concave up) above around 30 GHz. The similar results are obtained for the radio-data scaled by the relation of Vinyaikĭn (2014). If data taken from the second sample are used, similar results are obtained although the scatter is more prominent. The same conclusions hold if both scaling relations are used.

As the high-frequency radio-spectrum of Cas A is clearly curved, it is not appropriate to be fitted by the pure power-law. In the most simple case, it can be fitted by the two power-laws, below and above 30 GHz (excluding, of course, the low-frequency data influenced by the low-frequency cut-off). On the other hand, it is known that one of the

Table 1: Varying power-law best fitting parameters (0.55 - 353 GHz).

sample (scaling)	α	a	$\chi^2 (k)$	R^2
1 (Baars et al. 1977)	0.790 ± 0.016	0.056 ± 0.008	23.11 (34)	0.997
2 (Baars et al. 1977)	0.806 ± 0.016	0.062 ± 0.008	38.55 (42)	0.995
1 (Vinyaikĭn 2014)	0.841 ± 0.014	0.065 ± 0.007	27.33 (34)	0.997
2 (Vinyaikĭn 2014)	0.854 ± 0.013	0.069 ± 0.007	50.54 (42)	0.995

repercussions of non-linear effects of particle acceleration is the curved particle spectrum which in turn gives rise to the curved synchrotron spectrum (Ellison & Eichler 1984). In that sense, it is more appropriate to represent radio-spectrum of young SNRs with approximative relation that represents varying power-law of the form

$$S_{[\text{Jy}]}(\nu) = S_{[\text{Jy}]}(1\text{GHz}) \nu_{[\text{GHz}]}^{-\alpha+a \log \nu_{[\text{GHz}]}} \quad (4)$$

where α is the standard synchrotron spectral index and a is the parameter of spectral curvature which should be positive due to the non-linear behavior of DSA (Houck & Allen 2006; Vinyaikĭn 2014 and references therein). Of course, more general relation applied to the larger range of energies would include appropriate high-frequency synchrotron spectral cut-off which we do not take into account in this analysis.

The results of weighted least-square fits to data for this model applied to both samples and for different scaling relations are summarized in Table 1. Fit properties are given in form of χ^2 and R^2 defined as

$$\begin{aligned} \chi^2 &= \sum_{i=1}^N w_i (y_i - f(x_i; \beta_1, \dots, \beta_p))^2, \quad w_i = \frac{1}{\sigma_i^2}, \\ R^2 &= 1 - \frac{\chi^2}{TSS}, \\ TSS &= \sum_{i=1}^N w_i (y_i - \bar{y})^2, \quad \bar{y} = \frac{\sum_{i=1}^N w_i y_i}{\sum_{i=1}^N w_i}. \end{aligned} \quad (5)$$

In above relations, f is the predicted value from the fit, β_j are fit parameters ($j = 1, \dots, p$) and \bar{y} is the weighted mean of the observed data y_i at particular x_i , $i = 1, \dots, N$. w_i are the weights applied to each data point. TSS is the so called total sum of squares. It is worth stressing that in the case of non-linear models, the number of degrees of freedom is generally unknown, i.e. it is not possible to compute the value of reduced χ^2 or adjusted R^2 (Andrae et al. 2010). In Table 1, parameter $k = N - p$ is given for convenience. In non-linear models, k does not always represent the exact number of degrees of freedom (Andrae et al. 2010).

There are no significant differences in the fit results for both samples and for different scaling relations. Again, the exclusion of the data point at 353 GHz does not change the results significantly. It must be noted that the smoothly curved spectral shape represented by equation (4) gives a better fit than the model that assumes two power laws.

In Figure 2, the weighted least-square fit to the data from the first sample, for the varying spectral index model is presented. Scaling relation taken from Vinyaikĭn (2014) was used. Diamond symbols indicate *Planck's* data.

It is also appropriate to check if obtained values of above mentioned parameters, α and a , are consistent with the ones obtained when low-frequency cut-off is taken into account. To this end, the previous model was adjusted in the following way

$$S_{[\text{Jy}]}(\nu) = S_{[\text{Jy}]}(1\text{GHz}) \nu_{[\text{GHz}]}^{-\alpha+a \log \nu_{[\text{GHz}]}} e^{-\tau_0 \nu_{[\text{GHz}]}^{-2.1}}, \quad (6)$$

and is of the same form as the one stated in Vinyaikĭn (2014). τ_0 represents the optical depth at 1 GHz.

For this analysis new data samples were formed and analyzed. The third sample includes data from Tables 3 and 4 from Vinyaikĭn (2014) for the epoch 2015.5 as well as the *Planck's* data from Arnaud et al. (2014) appropriately scaled to match the same epoch.

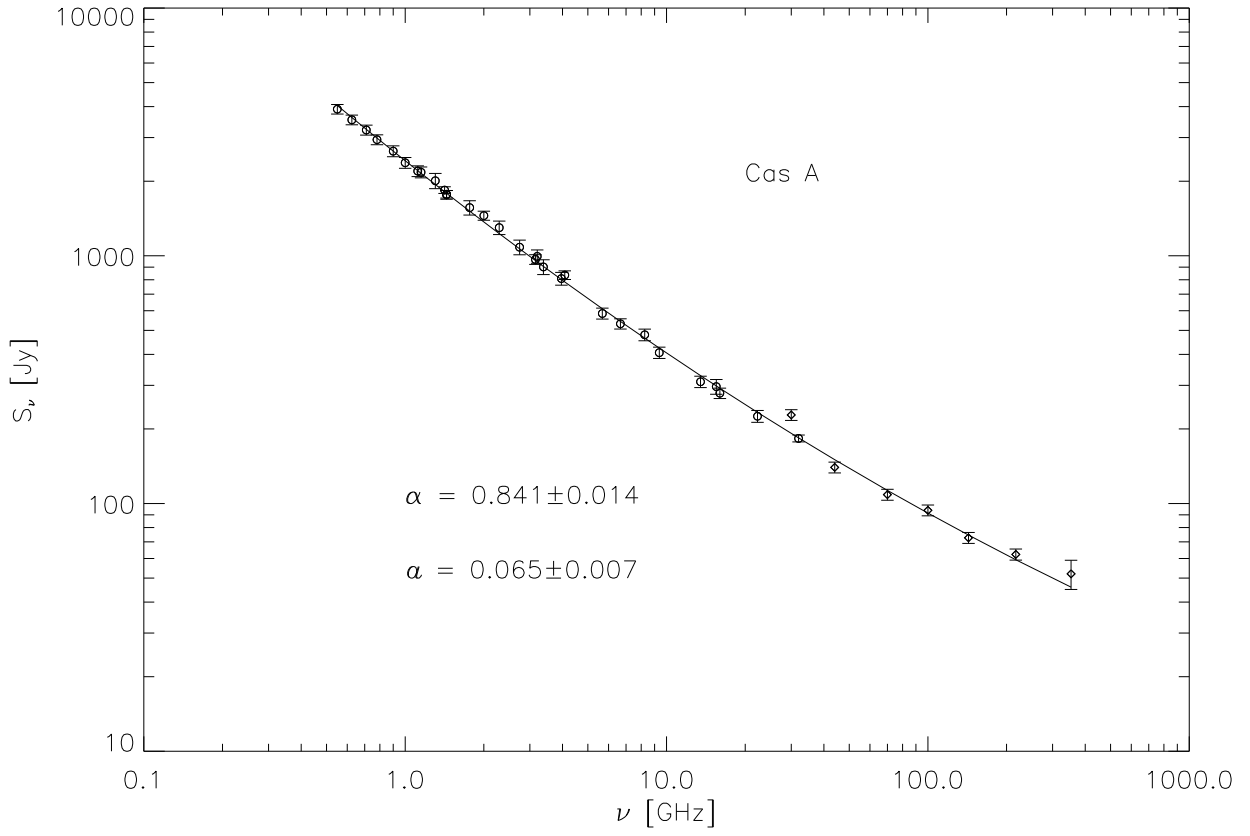


Fig. 2.— The weighted least-square fit to the data from the first sample, for the varying spectral index model. Scaling relation taken from Vinyaikin (2014) was used. Diamond symbols indicate *Planck's* data

The frequency range for this sample is 0.0056 - 353 GHz. The fourth sample includes all the data from Table 2 presented in Baars et al. (1977) with addition of data from Arnaud et al. (2014), Helmboldt & Kassim (2009) and Mason et al. (1999). Finally, the fifth sample incorporates the fourth one with the addition of data from Hurley-Walker et al. (2009) and Liszt & Lucas (1999). Data in fourth and fifth sample are scaled to the epoch of *Planck's* observations and the frequency range for these samples is 0.01005 - 353 GHz. In all these cases, scaling relation from Vinyaikĭn (2014) was only used.

The results of weighted least-square fits to data in this case are summarized in Table 2. There are no significant differences in the fit results for all samples. In Figure 3 the weighted least-square fit to the data from the fourth sample, for the varying spectral index model with low-frequency cut-off is presented. Diamond symbols indicate *Planck's* data.

The results are not significantly different than estimated in Vinyaikĭn (2014). On the other hand, the estimated values for spectral index around 1 GHz as well as for the curvature parameter are less than the ones obtained using the relation (4) on high frequency part of the radio-spectra alone.

The apparent excess radiation at 353 GHz, discussed in Arnaud et al. (2014), is also present in this analysis (see Figure 3). It may be due to the presence of cool dust in northern and western parts of Cas A (Dunne et al. 2009; Vinyaikĭn 2014). It should be noted that images at 600 GHz observed with the Herschel Space Observatory (Barlow

Table 2. Varying power-law with low-frequency cut-off best fitting parameters.

sample	frequency range [GHz]	α	a	τ_0	$\chi^2 (k)$	R^2
3	0.0056 – 353	0.762 ± 0.005	0.033 ± 0.003	$(7.738 \pm 0.574) \times 10^{-5}$	83.05 (29)	0.994
4	0.01005 – 353	0.760 ± 0.005	0.025 ± 0.003	$(8.968 \pm 0.869) \times 10^{-5}$	75.79 (46)	0.994
5	0.01005 – 353	0.765 ± 0.005	0.026 ± 0.003	$(9.209 \pm 0.875) \times 10^{-5}$	111.03 (54)	0.991

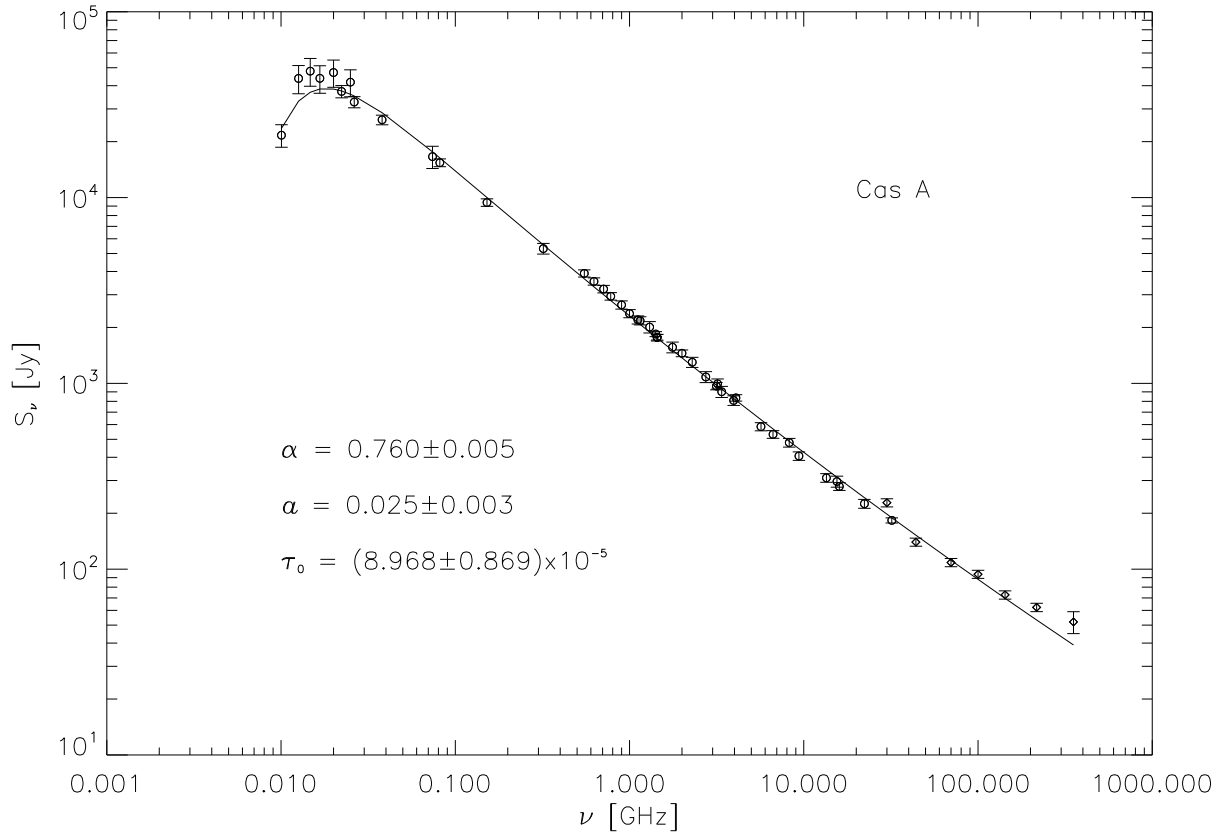


Fig. 3.— The weighted least-square fit to the data from the fourth sample, for the varying spectral index model with low-frequency cut-off. Diamond symbols indicate *Planck*'s data

et al. 2010) at much higher angular resolution than *Planck* ($6''$ - $37''$) show that the non-synchrotron microwave emission may be a combination of both cold interstellar dust and freshly formed dust. Arnaud et al. (2014) stressed that this excess could potentially be due to a coincidental peak in the unrelated foreground emission or to cool dust in the supernova remnant, which is marginally resolved by *Planck*.

The spinning-dust emission (electric dipole radiation from the rapidly rotating dust grains) could generally contribute significantly at high radio-frequencies, especially around 10 - 100 GHz (Draine & Lazarian 1998ab; Ali-Haïmoud et al. 2009; Scaife et al. 2007; Silsbee et al. 2011; Stevenson 2014). On the other hand, in the case of Cas A this emission component is negligible.

Finally, Vinyaikĭn (2014) showed that the observed slowing of the secular variations of the radio flux density of Cas A with decreasing frequency at decimeter wavelengths can be explained by a decrease in the optical depth of a remnant H II zone around Cas A with time due to recombination of hydrogen atoms. Due to the presence of the H II region it may be interesting to fit the radio spectrum of Cas A with the following expression

$$S(\nu) = S_1 \nu^{-\alpha} e^{-\tau\nu} + S_2 \nu^2 (1 - e^{-\tau\nu}),$$

$$\tau_\nu = \tau_0 \nu^{-2.1}. \tag{7}$$

This formula incorporates both synchrotron radiation as well as the thermal absorption and thermal bremsstrahlung emission from the zone in front of the synchrotron emitting region. Of course, this is a rather naive model. Supernova remnants are 3D structures, the fact that this relation does not take into account. On the other hand, it can serve as an approximative model for qualitative analysis.

If frequencies are in GHz then the (non-thermal) synchrotron flux density at 1 GHz is

simply $S^{\text{NT}}(1\text{GHz}) = S_1$ but for the thermal component holds

$$S^{\text{T}}(1\text{GHz}) = S_2 (1 - e^{-\tau_0}),$$

$$\Delta S^{\text{T}}(1\text{GHz}) = S^{\text{T}}(1\text{GHz}) \left(\frac{\Delta S_2}{S_2} + \Delta\tau_0 \frac{1}{e^{\tau_0} - 1} \right), \quad (8)$$

so that the contribution of thermal emission in integral radiation at 1 GHz is given by

$$\xi = \frac{S^{\text{T}}(1\text{GHz})}{S^{\text{T}}(1\text{GHz}) + S^{\text{NT}}(1\text{GHz})},$$

$$\Delta\xi = \xi \left(\frac{\frac{\Delta S^{\text{T}}(1\text{GHz})}{S^{\text{T}}(1\text{GHz})} + \frac{\Delta S^{\text{NT}}(1\text{GHz})}{S^{\text{NT}}(1\text{GHz})}}{1 + \frac{S^{\text{NT}}(1\text{GHz})}{S^{\text{T}}(1\text{GHz})}} \right). \quad (9)$$

The results of weighted least-square fits to data in this case are summarized in Table 3. Again, there are no significant differences in the fit results for all samples. The weighted least-square fit to the data from the fourth sample, for the test-particle synchrotron model with thermal absorption and emission is presented in Figure 4. Diamond symbols indicate *Planck's* data.

The presence of thermal emission from the H II region associated with this SNR is estimated to be around 1-2 % in the total flux density at 1 GHz. Addition of this component significantly improves fit to the data but discards the curvature due to non-linear effects of particle acceleration. It is worth noting that addition of the curvature parameter a to the previous model, i.e. varying power-law model with thermal absorption and emission in front

Table 3. Test-particle synchrotron model with thermal absorption and emission best fitting parameters.

sample	frequency range [GHz]	α	τ_0	ξ [%]	$\chi^2 (k)$	R^2
3	0.0056 – 353	0.769 ± 0.006	$(5.211 \pm 0.341) \times 10^{-5}$	1.653 ± 0.005	53.97 (29)	0.996
4	0.01005 – 353	0.785 ± 0.008	$(7.846 \pm 0.745) \times 10^{-5}$	1.913 ± 0.008	47.35 (46)	0.996
5	0.01005 – 353	0.788 ± 0.008	$(7.535 \pm 0.624) \times 10^{-5}$	1.887 ± 0.007	74.12 (54)	0.994

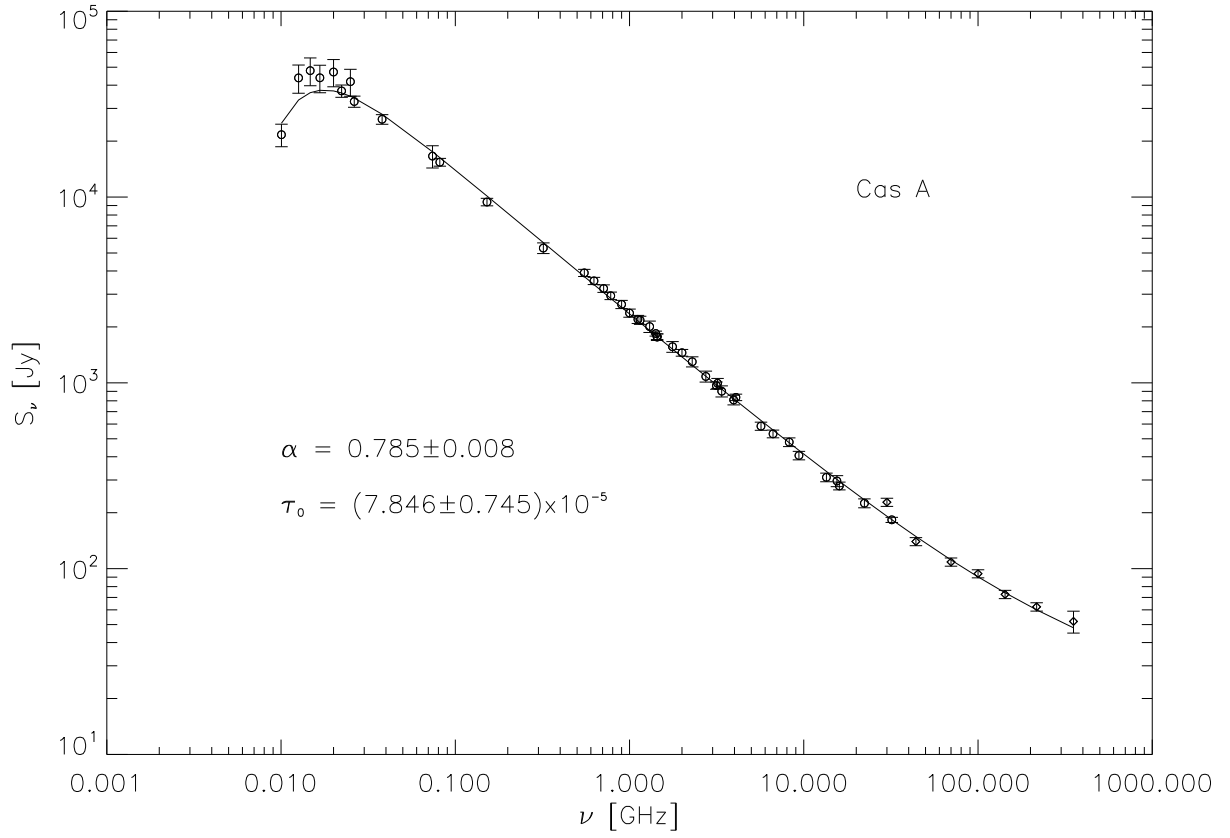


Fig. 4.— The weighted least-square fit to the data from the fourth sample, for the test-particle synchrotron model with thermal absorption and emission. Diamond symbols indicate *Planck's* data

of synchrotron emitting region, does not produce acceptable fits to all samples. Negative, i.e. non-physical in sense of the non-linear DSA effects², values for the curvature parameter a are preferred. Bounding the parameters to appropriate physical ranges of values do not improve fits that are also highly sensitive to initial guesses for the parameters. On the other hand, simple model represented by equation (7) fits to data very well (see Figure 4). The flux density estimate at 353 GHz is within the error bars of the measured value at this frequency for data samples 4 and 5 (see Figure 4).

3. Discussion

It is known that some young SNRs, such as Cas A and Kepler exhibit evidence of radio spectral variations from one region to another (Anderson & Rudnick 1996; DeLaney et al. 2002). This can lead to a curved composite spectrum even if the synchrotron spectrum for each region is just a power-law (Allen et al. 2008). On the other hand, the results of Jones et al. (2003) indicate that the spectra of particular small features in Cas A flatten with increasing energy and Allen et al. (2008) found that their results can be explained with model that includes curvature of particle spectra of $b = 0.06 \pm 0.01$. Curvature of particle spectra b is in fact four times spectral curvature a so that our results, although slightly

²When the pressure of cosmic-ray (CR) particles, produced at the shock wave, is included in the analysis, such a modification of shock structure implies changes in the spectrum of accelerated electrons. The energy spectrum of low energy electrons becomes softer (the radio spectrum is steeper) and the spectrum of high energy electrons becomes harder (the radio spectrum is shallower) than that of linear DSA. Due to significant CR production, the concave-up (positively curved) radio spectra is expected in the case of young SNRs (see Urošević 2014, and references therein for more details).

higher, are not in disagreement with conclusions of Allen et al. (2008).

For additional support to our claims, we used the same model for synchrotron radiation as in Allen et al. (2008), with one simplification that the non-thermal particle distribution function lacks high energy cut-off

$$N(E)dE = K \left(\frac{E}{E_0} \right)^{-\Gamma + b \log \frac{E}{E_0}}, \quad (10)$$

where $b = 4a$ is the curvature of particle spectra, $E_0 = 1$ GeV and Γ is particle spectral index at E_0 . Flux density is a combination of synchrotron radiation from such an ensemble and thermal absorption at low frequencies in a similar manner as in equation (6). The results, given in Table 4, show that the simplified model based on the one from Allen et al. (2008) is consistent with our previous results.

Finally, Dunne et al. (2009) showed that polarized sub-millimeter emission is associated with the SNR and that the excess polarized sub-millimeter flux at 353 GHz is due to cold dust within the remnant. They noted that there is no currently known way to produce such a polarized sub-millimeter emission from a synchrotron process.

Keeping in mind the fact that inclusion of thermal bremsstrahlung emission (equation 7) apparently leads to a better fit to data (Table 3), it must be noted that such an interpretation leads to a less contribution of dust emission at 353 GHz, which is in contrast

Table 4. Simplified model based on the one from Allen et al. (2008) best fitting parameters.

sample	frequency range [GHz]	α	a	τ_0	$\chi^2 (k)$	R^2
3	0.0056 – 353	0.775 ± 0.007	0.032 ± 0.001	$(8.032 \pm 0.500) \times 10^{-5}$	79.57 (28)	0.994
4	0.01005 – 353	0.739 ± 0.005	0.025 ± 0.003	$(8.998 \pm 0.867) \times 10^{-5}$	75.72 (45)	0.994
5	0.01005 – 353	0.777 ± 0.008	0.026 ± 0.003	$(9.268 \pm 0.872) \times 10^{-5}$	110.90 (53)	0.991

to the conclusion of Dunne et al. (2009). In that sense, we conclude that the more probable scenario is that *Planck's* new data actually reveal the imprint of non-linear particle acceleration in the case of this young Galactic SNR. Of course, we can not fully dismiss the possible contamination by adjacent H II region.

The additional attempt to support the non-linear particle acceleration hypothesis may come from the fit using non-linear synchrotron model with thermal absorption and dust Planck-like emission (Figure 5 and Table 5). To that end, the *Herschel's* total flux densities from Barlow et al. (2010) were added to data samples 3-5 forming samples 6-8. Again, similar results are obtained. Of course, this is a simplified model which does not distinguish between different dust emission components. On the other hand, the spectral curvature due to the non-linear particle acceleration is clearly present in this case too (see Table 5). These values for a are also more in accordance with the result of Allen et al. (2008).

It is also worth mentioning that Pohl et al. (2015) showed that stochastic re-acceleration of electrons downstream of the forward shock can explain the soft spectra observed from many Galactic SNRs. They also noted that, generally, interiors of the SNRs produce slightly steeper radio spectra than does the shell where re-acceleration occurs.

Table 5. The non-linear synchrotron model with thermal absorption and dust emission best fitting parameters.

sample	frequency range [GHz]	α	a	τ_0	$\chi^2 (k)$	R^2
6	0.0056 – 4285.714	0.756 ± 0.005	0.022 ± 0.004	$(6.807 \pm 0.579) \times 10^{-5}$	60.86 (33)	0.995
7	0.01005 – 4285.714	0.760 ± 0.005	0.020 ± 0.004	$(8.559 \pm 0.860) \times 10^{-5}$	69.55 (50)	0.994
8	0.01005 – 4285.714	0.764 ± 0.005	0.021 ± 0.003	$(8.800 \pm 0.865) \times 10^{-5}$	102.01 (58)	0.992

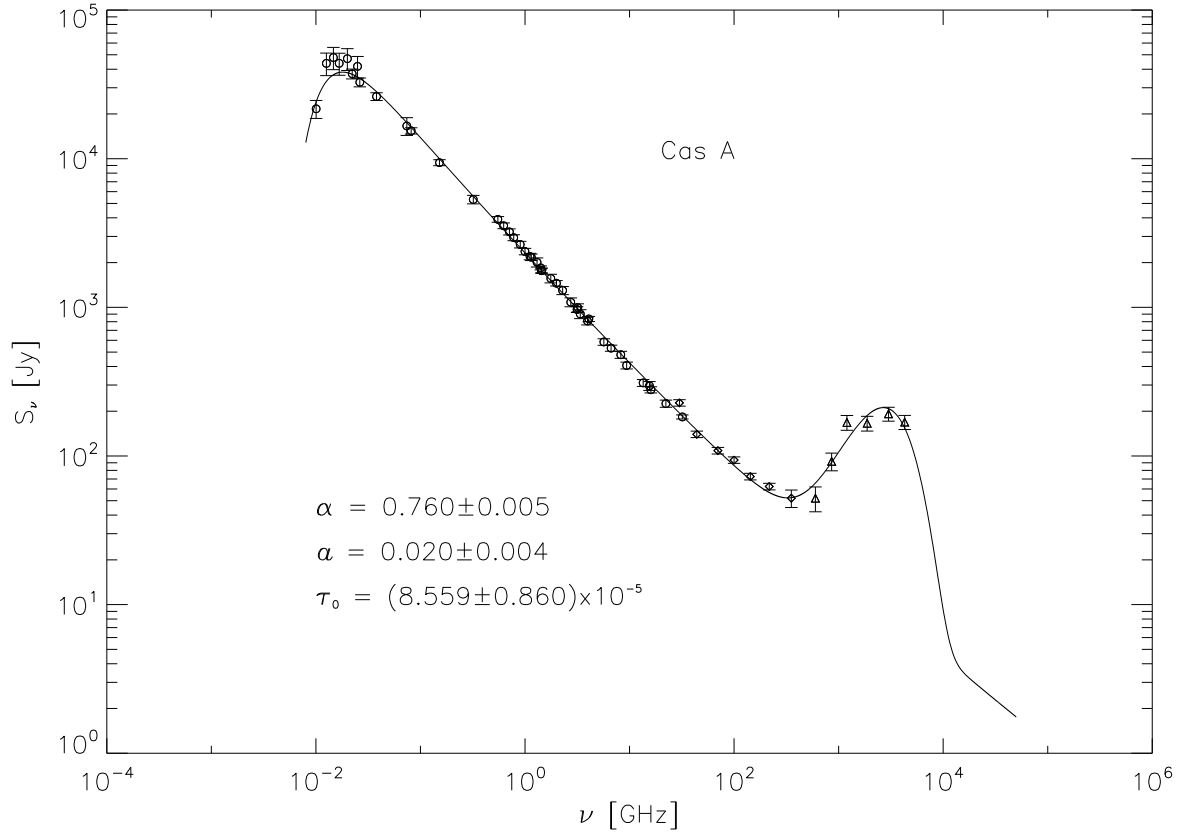


Fig. 5.— The weighted least-square fit to the data from the seventh sample, for the non-linear synchrotron model with thermal absorption and dust emission. Diamond symbols indicate *Planck's* and triangles *Herschel's* data

4. Conclusions

The main conclusions that can be drawn from this analysis are

(1) *Planck's* data support the observation that the radio continuum of SNR Cas A flattens with increasing frequency. The spectrum becomes positively curved above around 30 GHz.

(2) Alternative explanations of curvature are investigated: significant non-linear effects of particle acceleration, presence of thermal emission due to the emission of associated H II region, and the presence of dust emission.

(3) Different samples of data were analyzed to account for differences in data gathered from various literature. The presented results are not significantly sensitive to differences between samples.

(4) The results presented in this paper agree with the conclusions stated in Vinyaikĭn (2014), i.e. the observed flattening of the radio spectrum at millimeter wavelengths is most likely primarily due to a flattening of the radio synchrotron spectrum of Cas A itself. In other words, non-linear effects of particle acceleration are possibly mainly responsible for the apparent high-frequency curvature in Cas A radio spectrum.

We wish to thank the anonymous referee for useful suggestions which substantially improved this paper. This work is part of Project No. 176005 "Emission nebulae: structure and evolution" supported by the Ministry of Education, Science, and Technological Development of the Republic of Serbia.

REFERENCES

- Alarie, A., Bilodeau, A., & Drissen, L., 2014, MNRAS, 441, 2996
- Ali-Haïmoud, Y., Hirata, C., & Dickinson, C., 2009, MNRAS, 395, 1055
- Allen, G. E., Houck, J. C., & Sturmer, S. J., 2008, ApJ, 683, 773
- Anderson, M. C., & Rudnick, L., 1996, ApJ, 456, 234
- Andrae, R., Schulze-Hartung, T., & Melchior, P., 2010, arXiv 1012.3754A
- Arnaud, M. et al., 2014, arXiv 1409.5746P
- Ashworth, W. B., Jr., 1980, Journal for the History of Astronomy, 11, 1
- Baars, J. W. M., Genzel, R., Pauliny-Toth, I. I. K., & Witzel, A., 1977, A&A, 61, 99
- Babu, G. J., & Feigelson, E. D., 1996, Astrostatistics, Chapman & Hall
- Barlow, M. J., Krause, O., Swinyard, B. M., et al., 2010, A&A, 518, L138
- DeLaney, T., Koralesky, B., Rudnick, L., & Dickel, J. R., 2002, ApJ, 580, 914
- Draine, B. T., & Lazarian A., 1998a, ApJ, 494, L19
- Draine, B. T., & Lazarian A., 1998b, ApJ, 508, 157
- Dunne, L., Maddox, S. J., Ivison, R. J., Rudnick, L., Delaney, T. A., Matthews, B. C.,
Crowe, C. M., Gomez, H. L., Eales, S. A., Dye, S., 2009, MNRAS, 394, 1307
- Ellison, D. C., & Eichler, D., 1984, ApJ, 286, 691
- Fesen, R. A., Hammell, M. C., Morse, J., et al., 2006, ApJ, 645, 283

- Green D. A., 2014, 'A Catalogue of Galactic Supernova Remnants (2014 May version)',
Cavendish Laboratory, Cambridge, United Kingdom (available at
"http://www.mrao.cam.ac.uk/surveys/snrs/")
- Helmholtz, J. F., & Kassim, N. E., 2009, *AJ*, 138, 838
- Houck, J. C., & Allen, G. E., 2006, *ApJS*, 167, 26
- Hurley-Walker, N. et al., 2009, *MNRAS*, 396, 365
- Jones, T. J., Rudnick, L, DeLaney, T, & Bowden, J., 2003, *ApJ*, 587, 227
- Liszt, H., & Lucas, R., 1999, *A&A*, 347, 258
- Mason, B. S., Leitch, E. M., Myers, S. T, Cartwright, J. K., & Readhead, A. C. S., 1999,
ApJ, 118, 2908
- O'Sullivan, C., & Green, D. A., 1999, *MNRAS*, 303, 575
- Pohl, M., Wilhelm, A., Telezhinsky, I., 2015, *A&A*, 574, 43
- Reynolds, S., P., Ellison, D., C., 1992, *ApJ*, 399, L75
- Scaife, A., Green, D. A., Battye, R. A., et al., 2007, *MNRAS*, 377, L69
- Silsbee, K., Ali-Haimoud, Y., & Hirata C., 2011, *MNRAS*, 411, 2750
- Stevenson, M. A., 2014, *ApJ*, 781, 113
- Urošević, D., 2014, *Ap & SS*, 354, 541
- Vinyaikĭn, E. N., 2014, *Astron. Rep*, 58, 626